Available online at www.sciencedirect.com
ScienceDirect
Journal of Power Sources 161 (2006) 356–370
JOURNAL OF POWER SOURCES
www.elsevier.com/locate/jpowsour

Dynamic modeling of a methanol reformer—PEMFC stack system for analysis and design

Andrew T. Stamps, Edward P. Gatzke*

University of South Carolina, Department of Chemical Engineering, 301 Main St., Swearingen Eng. Ctr, Columbia, SC 29208, United States

Received 11 February 2006; received in revised form 30 March 2006; accepted 3 April 2006
Available online 9 June 2006

Abstract

Considerable effort has been devoted to the modeling of proton exchange membrane fuel cells (PEMFCs) as well as fuel processing units (FPUs). Many of these models consider only steady state analysis; the available dynamic models typically operate only in simple open loop configurations. However, a liquid fuel processor/PEMFC stack power unit for vehicular application will require tight integration and regulation of multiple units in order to function economically and reliably. Moreover, vehicular operation is inherently dynamic in nature, so traditional steady state process design approaches will be of limited value.

This work addresses a minimum set of subcomponents necessary for modeling an overall vehicular power system. Additionally, the integration and control of these sub-units is addressed so that the unit can be operated as needed in a vehicular application by following a reference power trajectory. A number of design and operational parameters can be adjusted and the impact on system performance studied. Based on this preliminary analysis, heuristics are developed for optimal operation and design.

Keywords: Liquid fuel reformer; PEMFC stack modeling; System modeling

1. Introduction

Dwindling supplies of fossil fuels have caused researchers and policy makers to explore alternative energy sources. As of 2003, energy consumption by the transportation sector comprised 27% of total US energy consumption and 67% of all US petroleum consumed [1]. Consequently, one of the largest alternative energy research initiatives lies in transportation technology. Developing technologies that reduce the demand on petroleum products has environmental benefits from reduced consumption in addition to economic and political benefits from the reduced dependence on foreign oil imports. Despite continued improvements in engine and fuel injection technology, which have increased the average fuel economy of passenger vehicles from 13.5 miles per gallon (mpg) in 1970 to 22.1 mpg in 2002, both the total number of vehicles and the average annual distance travelled per vehicle have steadily increased over the same time period. The net result is an approximately 70% increase in the amount of motor fuel consumed [1].

Even considering improved fuel economy, current internal combustion engines (ICEs) achieve an energy efficiency of approximately 20% [48]. Further efficiency increases are unlikely without significant modifications and technological breakthroughs. Therefore, a significant amount of research has been directed towards alternative fuel technologies, such as hybrids, plug-in hybrids, and fuel cell vehicles (FCVs). Hybrids combine a small ICE with a battery system connected to an electric motor/generator. While the vehicle is powered largely by the ICE, the electric motor provides supplemental power from the battery pack during high-load conditions such as acceleration. During lower load conditions such as idling or cruising, surplus power produced by the ICE drives the electric motor which is then operated in reverse as a generator to recharge the batteries. Likewise, regenerative braking techniques can be employed during deceleration to recover some of the kinetic energy of the vehicle, converting it back to electrical energy stored in the batteries. Since these vehicles incorporate already existing ICE technology, they have reached a more advanced stage of development with a number of models such as the Toyota Prius, Honda In-

* Corresponding author. Tel.: +1 803 777 1159; fax: +1 803 777 8265.
E-mail address: gatzke@sc.edu (E.P. Gatzke).

0378-7753/$ – see front matter © 2006 Elsevier B.V. All rights reserved.
doi:10.1016/j.jpowsour.2006.04.080

Nomenclature

A_{mem} PEMFC stack membrane area for each cell (cm^2)
c total molar concentration of gaseous species in methanol reformer ($mol\,m^{-3}$)
c_i molar concentration of species i in methanol reformer ($mol\,m^{-3}$)
$c^*_{O_2}$ saturation concentration of oxygen in the PEMFC membrane ($mol\,m^{-3}$)
C capacitance of PEMFC stack (F)
C_{aux} auxiliary power capacity (A h at 120 V)
C_p constant pressure heat capacity ($J\,mol^{-1}$ or $J\,kg^{-1}$)
$C_{p,cat}$ Heat capacity of catalyst bed in reformer ($J\,kg^{-1}$)
$C_{p,gas}$ Heat capacity of reformer gas ($J\,mol^{-1}$)
E_s energy in PEMFC stack body (J)
$\dot{E}_s$ rate of change of energy in PEMFC stack body ($J\,min^{-1}$)
Eq_j Equilibrium driving force of reaction j in methanol reformer
$\mathcal{F}$ Faraday constant ($C\,mol^{-1}$)
h channel height in cross-flow heat exchanger (m)
(hA) lumped convective heat transfer rate ($J\,min^{-1}\,K$)
H_i specific enthalpy of species i ($J\,kg^{-1}$)
$\Delta H_{rxn,\,j}$ heat of reaction j in methanol reformer ($J\,mol^{-1}$)
i current density in PEMFC stack ($A\,cm^{-2}$)
I current in PEMFC stack (A)
k_j rate constant for reaction j in methanol reformer ($mol\,m^{-3}\,min^{-1}\,kPa$)
k_v valve proportionality constant ($m^3\,min^{-1}\,atm$)
K_{aux} auxiliary power recharging proportionality constant ($W\,A^{-1}\,h$)
K_c PI controller gain
$K_{eq,j}$ equilibrium constant of reaction j in methanol reformer (kPa^x)
L_x length of cold channel in cross-flow heat exchanger
L_y length of hot channel in cross-flow heat exchanger
m_i mass of species i (kg)
$\dot{m}_i$ mass flow rate of species i ($kg\,min^{-1}$)
M_i molecular weight of species i ($kg\,mol^{-1}$)
N number of cells in PEMFC stack
P_{an} pressure in anode channel of PEMFC stack (atm)
P_{ca} pressure in cathode channel of PEMFC stack (atm)
$P_{desired}$ desired system power level (W)
P_i partial pressure of species i in the reformer (kPa)
P_{sp} PEMFC stack power setpoint (W)
P_{stack} PEMFC stack power (W)
ΔP pressure drop across a valve (atm)
$\dot{q}$ heat flux ($J\,m^{-2}\,s$)
$\dot{Q}_{cool}$ cooling rate on PEMFC stack ($J\,min^{-1}$)
r_j reaction rate of reaction j in methanol reformer ($mol\,m^{-3}\,min$)
R ideal gas constant ($J\,mol^{-1}\,K$)
R_{act} cell resistance due to oxygen activation losses (ohm)
R_{ohm} cell resistance due to transport (Ohmic) losses (ohm)
R_r radius of reformer reactor (m)
s Laplace domain variable
t time (min)
T methanol reformer temperature (K)
T_{wall} external wall temperature of methanol reformer (K)
v_z gas velocity in axial direction of methanol reformer ($m\,min^{-1}$)
U convective heat transfer coefficient ($J\,m^{-2}\,s\,K$)
$\dot{V}$ volumetric flow rate ($m^3\,min^{-1}$)
V_{act} Dynamic activation overvoltage (V)
V_{cell} voltage of a single cell within the PEMFC stack (V)
V_{stack} PEMFC stack voltage (V)
z axial dimension of methanol reformer (m)

Greek symbols

γ overall volume fraction of methanol reformer
Γ_x weighting factor for objective x in multiobjective optimal design framework
ϵ porosity of catalyst pellets in methanol reformer
ϵ_{bed} void fraction of packed catalyst bed in methanol reformer
η_{act} steady state activation overpotential in PEMFC cell (V)
η_{eff} reaction effectiveness factor in methanol reformer
ν_i stoichiometric coefficient of species i in PEMFC stack reactions
ξ_x emperical modeling coefficient in PEMFC stack model
ρ density ($kg\,m^{-3}$)
ρ_{cat} bed density of packed catalyst pellets ($kg\,m^{-3}$)
τ_f First order filter time constant (min)
τ_I PI controller integral time constant (min)
φ_x cost of objective x in multiobjective optimal design formulation
Φ multiobjective optimal design cost function

sight, Honda Civic hybrid, Honda Accord hybrid, and the Ford Escape hybrid already commercially available and rapidly gaining popularity. Fuel economies range from 29 mpg (city) for the high-power Honda Accord hybrid to 66 mpg (highway) for the Honda Insight, according to EPA estimates. Regardless of the model, fuel economy is significantly higher than the current national average.

Plug-in hybrids are similar in many respects to conventional hybrids, except they feature a smaller ICE with a larger electric motor/generator and battery pack. As the name implies, plug-in hybrids will need to connect to an external electrical source to charge the battery pack completely. When fully charged, plug-in

hybrids will operate entirely on electrical power until the power level in the battery pack drops to a certain level. It is expected that they will be able to drive 20–35 miles on batteries alone before the ICE is required. Once the ICE starts, operation will be more similar to a traditional hybrid with power control system only recharging the batteries enough from the ICE to maintain hybrid operation. Once the operator reaches a destination with proper charging equipment, the vehicle can be plugged-in and the batteries fully recharged. Given standard driving habits, this operational paradigm could result in a large percentage of transportation energy coming from electricity rather than petroleum fuels, in addition to the higher fuel economy of hybrid electric vehicles. Some estimates have placed the reduction in oil for transportation by as much as 74% – assuming full market penetration – by switching to the plug-in hybrid configuration [48].

Both traditional hybrids and plug-in hybrids offer significant improvements over traditional ICE vehicles in terms of fuel economy, but still require gasoline or diesel fuel. In order to entirely eliminate the need for fossil fuels, another prominent research area involves the use of hydrogen as fuel. Although it is possible to combust hydrogen in a traditional ICE, significant effort has been devoted to fuel cells, particularly proton exchange membrane fuel cells (PEMFCs), which oxidize hydrogen electrochemically to produce electrical power. Due to the lower operating temperature of PEMFCs, it is believed that the energy efficiency of hydrogen fuel cell powered vehicles can exceed 40%. While the ideal fuel source for fuel cells is pure hydrogen, there are a number of technological, economic, and infrastructure-related hurdles that make it unlikely that the first commercially-available FCVs will run directly on compressed gaseous or liquid hydrogen. Instead, early FCVs will likely be fueled by liquid hydrocarbons such as methanol (MeOH), ethanol (EtOH), gasoline, or naphtha, which is then converted on-board into a hydrogen-rich fuel stream [49]. While it would be convenient to continue to use gasoline as a hydrogen source for FCVs [18], environmental concerns over greenhouse gas emissions will likely dictate a switch to lighter hydrocarbons such as methanol or ethanol which offer a higher ratio of hydrogen to carbon dioxide. In fact, the reforming of methanol can yield a hydrogen to carbon dioxide ratio as high as 3:1, whereas the partial oxidation of octane (as an approximation for gasoline) can only achieve a maximum ratio of 9:8. Due to the relatively high hydrogen/carbon ratio of methanol, several groups have begun studying methanol reforming specifically for the production of hydrogen for PEMFC applications [7,27,30].

Considerable work has already been done to develop FCVs running directly on pure hydrogen. GM, Daimler-Chrysler, BMW, and others have working prototypes. However, the research and design is at a much earlier stage for vehicles that feature on-board hydrogen production from liquid fuels. Overall, the systems will be considerably more complicated, since the equipment needed to convert the liquid fuel to hydrogen-rich gas and likely purify it has its own set of energy demands and dynamic behaviors. Not surprisingly, a number of design considerations will impact the cost and efficiency of such a plant as well as its operability and controllability. One major concern is start-up time: how long will it take for a reformer to heat to operating temperature and begin producing enough hydrogen to run the fuel cell? The cold start of methanol reformers is currently under investigation and strategies are being developed to minimize warm-up time [28,15]. Nevertheless, in order to "turn the key and go", FCVs will likely require battery networks similar to today's gasoline-electric hybrids in order to power the vehicle while the hydrogen production and fuel cell systems come online.

Additionally, heat integration will be crucial to the overall efficiency of the vehicle. The fuel cell itself generates excess heat, and depending on the type of liquid fuel conversion, that process may be at elevated temperature as well. In order to increase efficiency, some of this heat may be recovered by using it to preheat the feed stream to the reformer unit as well as the air feed to the cathode. However, this sort of integration couples the dynamics of various units and could lead to unforeseen behaviors under transient driving conditions. Therefore, it is important to closely study the design and integration of any combined liquid fuel processor and fuel cell stack system not only from a steady state perspective, but from a dynamic one as well.

The following work is divided into several sections. First, the development and implementation of the core components within the overall system model is discussed. This is followed by the assembly of the components into a complete system model and a description of the necessary control loops for dynamic power-level operation. Using the system structure presented, design sensitivity studies were performed and the results examined. Finally, future directions for this work are considered.

2. Component modeling

The liquid-fueled PEMFC power plant is by design a combination of subsystems coupled together. In order to study the behavior of the system as a whole, it is necessary to have appropriate models of all constituent components. At the very minimum, models for the PEMFC stack and a fuel processing unit are required. Ultimately, the fuel processing unit will itself be comprised of several sub-units including reforming, water-gas shift, and preferential oxidation reactors or reaction zones within a single reactor. This complicated arrangement is necessary to reduce the amount of CO and other PEMFC catalyst poisons present in the reformate stream. However, in an effort to reduce the complexity of the overall system model, a single model of a methanol reformer is used individually as the fuel processing unit (FPU). Since the reforming reaction is endothermic, the dynamics of the reformer should be the slowest of all the components within the fuel processor, and thus should be a good indicator of the behavior of the fuel processing unit as a whole.

A model for the PEMFC stack is the other critical component. While very sophisticated models have been developed for various fuel cells and stacks [20,45,22], their computational cost is quite large and generally prohibitive for dynamic studies, particularly at the system level. The desire for this work is to have a relatively simple model that provides a reasonably accurate account of the overall material and energy flows of the system as well as the voltage behavior of the stack as a whole in an

efficient manner. A suitable model has been adapted from the literature to accomplish these goals [51,38].

Finally, a variety of ancillary equipment is required to build an actual system. This includes pumps, burners/heaters, blowers, heat exchangers/evaporators, auxiliary power sources, and power controllers/converters. However, many of these items add needless complexity to the model while providing minimal additional insight into the process. Nevertheless, two items from this list bear further discussion. The reformer and PEMFC stack operate at considerably different temperatures and so it becomes necessary to cool, heat, and evaporate various process streams at different points to operate safely and efficiently. Therefore, there is the opportunity for heat integration to use one stream to heat or cool a second in the process. This heat integration more tightly couples the operation of all units, but should ultimately allow for a higher energy efficiency for the system. Hence, there is a need for some basic heat exchanger modeling to examine the effects of different heat integration schemes.

In addition to the heat exchangers, the role of the auxiliary power supply is also important. By examining the amount of auxiliary energy and power needed to operate a particular system configuration, one can determine what type and size of auxiliary power source is needed. From that data, economic, size, and weight constraints may dictate whether a particular design is practical. A more detailed treatment of each component is presented below.

2.1. Methanol reformer

2.1.1. Modeling assumptions

In order to clarify development and speed computation, a number of modeling assumptions and simplifications have been made. One significant assumption is that the reactor behaves as if it is plug-flow. Therefore, the only spatial gradients in this model will be in the axial direction along the length of the reactor. Given the relatively large flow rate and the packed-bed conditions inside the reactor, this should provide a reasonable approximation. It is also assumed that all chemical components remain in the gas phase, so that the system can be modeled as a single phase. Furthermore, the gasses are assumed to obey the ideal gas law in order to avoid the solution of nonlinear equations of state at each step of integration. This is a reasonable assumption, considering the operating conditions of this reactor with temperatures greater than 200 °C and pressures well below 10 atm. A constant pressure assumption is made for the sake of simplicity. By using the constant pressure assumption together with the ideal gas law and an assumption of no spatial gradients in mass flux, the superficial velocity can be identified as a function of position.

Finally, the heat transfer in the reactor must be considered. For a reactor with pressure driven flow, it is reasonable to assume that the Péclet number, the ratio of convective heat transfer to conductive heat transfer: $\frac{\rho C_p v L}{k}$, is quite large, so conduction within the gas and between the gas and the solid catalyst pellets is neglected. Additionally, the catalyst bed is assumed to have the same temperature distribution as the gas flowing through it. The transfer of heat into the reactor from the surroundings is treated empirically as convective heat transfer using Newton's law of cooling, which states that the heat flux into the reactor is proportional to the difference between the gas temperature inside the reactor and the specified external wall temperature given in the following equation:

$$\dot{q}(z) = U(T_{\text{wall}} - T(z)) \tag{1}$$

The parameter U is the heat transfer coefficient which is either determined experimentally or through an experimental correlation such as the Colburn analogy [16]. Values will typically be in the range of 25–100 J m^{-2} s^{-1} K. For the purpose of this model, it is assumed that the external wall temperature is uniform and can be maintained at a desired temperature by a heating element. In practice, the heat will likely be provided by the catalytic combustion of methanol and/or the hydrogen remaining in the anode off gas. The utilization of the excess hydrogen in the off gas will be part of the heat integration process and critical to the overall fuel efficiency of the vehicle.

2.1.2. Reaction network and kinetics

Given the current interest in hydrogen production from liquid fuels such as methanol, a number of studies have recently appeared in the literature characterizing various types of catalysts for the numerous routes of hydrogen production from methanol. These studies include methanol decomposition, steam reforming, partial oxidation, and combined/autothermal/oxidative methanol reforming—a combination of steam reforming and partial oxidation. Additionally, several novel reactor configurations have been proposed with improved heat and mass transfer properties over traditional packed-bed reactors.

Of all the potential catalysts studied, Cu and mixtures of Cu/ZnO on Al_2O_3 have received the most attention [34,47,40,39,2,3,12]. These catalysts have been in use commercially for several decades in the synthesis of methanol. With the addition of water as a reactant, they work very well to catalyze the steam reformation of methanol to produce H_2 and CO_2 with a high conversion of methanol and a high selectivity to H_2 and subsequent low selectivity towards CO. This is particularly important for PEM fuel cell applications, since CO is a poison to the proton exchange catalysts even at very low concentrations. One of the reasons for the low selectivity towards CO is that the catalyst also facilitates the water-gas shift reaction:

$$\text{CO} + \text{H}_2\text{O} \longleftrightarrow \text{CO}_2 + \text{H}_2 \tag{2}$$

which is driven towards the right with a stoichiometric excess of water. However, steam reforming is a relatively endothermic reaction ($\Delta H_{\text{rxn}} = 49\ \text{kJ mol}^{-1}$) which requires an external source of heat, a definite design hurdle for a portable application such as a fuel cell vehicle. To make matters worse, these catalysts exhibit slow reaction rates and therefore need to operate at temperatures exceeding 250 °C. This combination of factors makes traditional packed-bed reactors using these catalysts thermally sluggish, which in turn makes it difficult to respond to rapid changes in load.

Others such as Agrell et al. [2] have examined the effects of using zirconia (ZrO_2) as an alternate (or additional) support ma-

terial for Cu/ZnO with some performance gains during steam reformation. However, these catalysts exhibited a higher light-off temperature and elevated CO production compared to the Al_2O_3 only catalysts when used in an oxidative steam reforming environment. Moving away from steam reforming entirely, others have discussed direct and oxidative decomposition of methanol on Pd/SiO_2 (references contained in [23]) and the use of indium tin oxide/alumina (ITO/Al_2O_3) for the partial oxidation of methanol (POM) [29], shown in the following equation:

$$MeOH + \tfrac{1}{2}O_2 \longrightarrow 2H_2 + CO_2 \quad (3)$$

Direct decomposition of methanol is impractical for portable fuel cell purposes, in that it is both highly endothermic ($\Delta H_{rxn} = +90.6\,kJ\,mol^{-1}$) and it produces a large amount of CO as a product. Conversely, POM is highly exothermic ($\Delta H_{rxn} = -192\,kJ\,mol^{-1}$) which makes it difficult to control. Additionally, the maximum yield of H_2 is only 2 mol mol^{-1} MeOH with POM compared to a possible 3 mol mol^{-1} MeOH with steam reforming, with a fairly significant production of CO as a byproduct. Thus, the most promising technique for hydrogen generation for portable PEM fuel cell applications is oxidative steam reforming of methanol (OSRM), also known as combined steam reforming (CSR) or autothermal reforming, when the system is operated adiabatically. In addition to the water and methanol needed for steam reforming, a sub-stoichiometric amount of O_2 (or air) is added to the feed so that some methanol is consumed by the POM pathway. The overall OSRM reaction is given by:

$$MeOH + (1-x)H_2O + \tfrac{1}{2}xO_2 \longrightarrow (3-x)H_2 + CO_2 \quad (4)$$

where x is the fraction of methanol consumed by the POM mechanism [30]. Consequently, the overall heat of reaction for OSRM depends on x and is given by $\Delta H_{rxn} = 49.5 - 241.5x\,kJ\,mol^{-1}$. Adjusting reaction conditions so that $x \approx 0.2$ results in an adiabatic or autothermal system in which the overall energy change is neutral. There are numerous advantages to OSRM (see Turco et al. [47] and references therein). (i) The heat released by the POM is used to drive the reforming reaction. When the O_2 (air) stream is regulated properly, no additional heat will be need to be added to the reactor to sustain operation; (ii) By using the excess heat of POM for steam reforming, the reactor temperature is more easily controlled than an exothermic POM reactor and responds to transients more quickly than an endothermic reformer; (iii) The presence of water in the system drives the water-gas shift reaction towards H_2 and CO_2 which helps eliminate the CO produced from incomplete oxidation in the POM pathway; (iv) OSRM has a slightly lower H_2 yield than traditional steam reforming, but the elimination of the need for an exogenous heat supply and improved dynamic response makes up for this loss. Moreover, the yield is still noticeably better than POM alone.

Unfortunately, very little information is available in the literature about the overall kinetics of OSRM. In order to prototype the design methodology, it was decided to focus on steam reforming, for which more quantitative information exists. For the present version of the model, the kinetics of the reformation of methanol were obtained from Mizsey et al. [34]. The reaction network was given as follows:

$$MeOH \longleftrightarrow CO + 2H_2 \quad (+90.6\,kJ\,mol^{-1})$$

methanol decomposition (D) (5)

$$CO + H_2O \longleftrightarrow CO_2 + H_2 \quad (-41.1\,kJ\,mol^{-1})$$

water-gas shift (W) (6)

$$MeOH + H_2O \longleftrightarrow CO_2 + 3H_2 \quad (+49.5\,kJ\,mol^{-1})$$

steam reforming (R) (7)

Each of these reactions has an experimentally-determined, temperature-dependent equilibrium constant, given by the following equations:

$$K_{eq,D} = 1.718 \times 10^{14} \exp\left(-\frac{95418}{RT}\right) \quad (8)$$

$$K_{eq,W} = 9.543 \times 10^{-3} \exp\left(\frac{39876}{RT}\right) \quad (9)$$

$$K_{eq,R} = 1.849 \times 10^{10} \exp\left(-\frac{56087}{RT}\right) \quad (10)$$

Using the equilibrium coefficients, equilibrium driving force expressions can be developed:

$$Eq_D = 1 - \frac{P_{CO} P_{H_2}^2}{K_{eq,D} P_{MeOH}} \quad (11)$$

$$Eq_W = 1 - \frac{P_{CO_2} P_{H_2}}{K_{eq,W} P_{CO} P_{H_2O}} \quad (12)$$

$$Eq_R = 1 - \frac{P_{CO_2} P_{H_2}^3}{K_{eq,R} P_{MeOH} P_{H_2O}} \quad (13)$$

Finally, the overall rate expressions for the three reactions are given by:

$$r_D = k_D P_{MeOH} Eq_D \quad (14)$$

$$r_W = k_W P_{CO} Eq_W \quad (15)$$

$$r_R = k_R P_{MeOH} Eq_R \quad (16)$$

where the rate constants k_x are assumed to obey the Arrhenius temperature dependence with activation energy and pre-exponential factors given in Table 1. It should be noted that this reaction mechanism was determined with water in excess. Additionally, this mechanism does not incorporate the methanol oxidation pathway, which is required for autothermal methanol reforming.

Table 1
Arrhenius parameters for methanol decomposition (obtained from Mizsey et al. [34])

Reaction	Activation energy ($kJ\,mol^{-1}$)	Pre-exponential factor ($mol\,g\,cat^{-1}\,s^{-1}\,kPa^x$)
Methanol decomposition	76(±4%)	1.12(±12%)
Water-gas shift	50(±25%)	0.0023(±32%)
Steam reforming	81(±7%)	6.75(±34%)

Note that by adding the stoichiometric coefficients of the decomposition and water-gas shift reactions, one obtains the stoichiometry of the steam reforming reaction. Thus, this system is not actually three independent reactions. Since only two of the three reactions are linearly independent, only two of the species reaction rates are distinct and the remainder are expressed as a combination of the first two as demonstrated in the following equations:

$$r_{CO_2} = r_W + r_R \tag{17}$$

$$r_{CO} = r_D - r_W \tag{18}$$

$$r_{H_2O} = -r_{CO_2} \tag{19}$$

$$r_{MeOH} = -(r_{CO_2} + r_{CO}) \tag{20}$$

$$r_{H_2} = 3r_{CO_2} + 2r_{CO} \tag{21}$$

2.1.3. Model equations

The model equations for this system consist of the standard multi-component mass and energy balances for cylindrical, plug-flow geometry with corresponding modifications for the packed nature of the bed and the form of heat transfer into the reactor. A void fraction ϵ_{bed} is specified, which denotes what amount of the bed is unoccupied by pellets. Values of the void fraction vary widely based on the size and geometry of the packing material. However, for packed-bed catalytic reactors, values of 0.3–0.5 are common [21]. The methanol reforming reactor used by Dams et al. [17] is estimated to be 0.37. Additionally, the ratio of pore volume to total pellet volume is the porosity, denoted ϵ. By combining the void fraction and pellet porosity, the volume fraction γ available to the gas within the reactor is given by the following equation:

$$\gamma = \epsilon_{bed} + (1 - \epsilon_{bed})\,\epsilon \tag{22}$$

At this point, one may start from very general mass and energy balances and begin simplifying as demonstrated in Nauman, pp. 531–533 [35]. However, this particular analysis has been performed previously for the methanol reforming system by Dams et al. [17], giving rise to the component mass balance:

$$\gamma \frac{\partial c_i}{\partial t} + \epsilon_{bed} \frac{\partial}{\partial z}(v_z\, c_i) = \eta_{eff}\, \rho_{cat}\, r_i \tag{23}$$

and the energy balance:

$$(\gamma c C_{p,gas} + \rho_{cat} C_{p,cat}) \frac{\partial T}{\partial t} + \epsilon_{bed} v_z c C_{p,gas} \frac{\partial T}{\partial z} = 2\frac{U}{R_r}(T_{wall} - T) - \eta_{eff}\, \rho_{cat} \sum_{j \in \{D,W,R\}} \Delta H_{rxn,j}\, r_j \tag{24}$$

In Eqs. (23) and (24) above, c_i is molar concentration of species i, while c is the molar concentration of all gaseous species. Additionally, η_{eff} is the effectiveness factor which can be used to account for mass transfer limitation of the rate of reaction within the pellet; $C_{p,gas}$ is the molar heat capacity (J mol^{-1} K^{-1}) of the gas phase; $C_{p,cat}$ is the specific heat capacity (J kg^{-1} K^{-1}) of the catalyst pellets; ρ_{cat} is the packed density of the catalyst pellets; R is the radius of the reactor tube. Finally, $\Delta H_{rxn,j}$ is the heat of reaction for the jth reaction pathway in the system. Combined with the ideal gas law:

$$c_i = \frac{P_i}{RT} \tag{25}$$

this completes the modeling of the packed-bed methanol reformer.

2.1.4. Implementation

The governing mass and energy balances for the reformer are partial differential equations (PDEs) with a single spatial dimension. Very few nonlinear PDEs have analytical solutions, so it becomes necessary to rely on numerical techniques. A variety of methods exists for the numerical solutions of different classes of PDEs. The reformer model consists of six coupled parabolic PDEs with a simple linear geometry, so techniques such as collocation, finite differences, and the method of lines would be suitable solution strategies. The method of lines uses finite differences to discretize the spatial derivatives across a domain of interest, thereby converting a system of PDEs into a larger system of coupled ordinary differential equations (ODEs) depending only on time [42]. Many robust algorithms and packages exist for solving systems of ODEs [32,33,26,41], which generally makes this method more reliable than a pure finite difference approach where both spatial and temporal derivatives are discretized. Since the time derivatives of Eqs. (23) and (24) can be isolated algebraically, this system is an excellent candidate for solution through the method of lines.

It was determined that at least 50 discretization intervals were required to sufficiently reduce spatial discretization error, which results in a system of 300 coupled ODEs (6 states at 50 points). Given the large number of equations, the system was implemented in a compiled language using the integration routine LSODA [26,41] that can efficiently accommodate the banded structure of the system. When the reformer model is simulated in a native code environment (C linked to LSODA in Fortran), the same simulation that took 200 s using the Matlab® stiff system solver `ode23s` completes in about 0.1 s. However, adjusting model parameters, changing simulation protocols, and manipulating the simulation output are all more cumbersome in a purely native code environment. Therefore, the external C-language API for Matlab® was utilized to create an interface between Matlab®/Simulink® and the compiled reformer model/LSODA solver. This allows for easier manipulation of parameters and creation of simulation protocols. Additionally, the simulation output can be directly accessed and plotted within Matlab®. The simulation of the model through this interface does add some computational overhead, extending simulation time to 0.7 s, but the utility and ease-of-use outweighs the performance drop over native code while still providing substantial improvement over a pure Matlab®/Simulink® implementation. With its relatively high fidelity and an execution time of <1 s, this model is an excellent candidate to use for in an optimal design framework.

2.1.5. Model validation

The report by Dams et al. [17] contains data from several experimental trials, which is useful for calibrating the reformer model developed above. Experiments were performed in which the external heating was adjusted alone or simultaneously with feed flow adjustments. Their test unit was a stainless steel reactor bed 45 cm long and 5.2 cm in diameter, corresponding to an internal volume of approximately 1 L. It was filled with 1.5 kg of ICI 33–5*A* $Cu/ZnO/Al_2O_3$ low-temperature shift catalyst. The outer wall was wrapped with a 600 W electrical heating tape and covered with insulating material to reduce heat loss to the surroundings. The feed to the reformer consisted of a 3:2 mixture (volume basis) of methanol and water, a methanol weight fraction of 0.542. The liquid feed was vaporized and superheated prior to injection in order to prevent condensation upon entry to the catalyst bed. Since PEMFCs operating on reformate are expected to run at elevated anode pressures, the reformer was maintained at 30 psig, even though elevated pressure favors the production of CO instead of H_2.

Several steps were necessary to fit the data. The experimental system varied the power level in the heating tape, whereas the model assumes that heat is applied through the variation of wall temperature. Since a change in heater power does not produce an instantaneous change in wall temperature, the model approximates the experimental conditions by passing any wall temperature changes through a first-order lag, with a filter time constant adjusted to fit the data. Ultimately, the fitting procedure was an iterative process. First the wall temperature changes and heat transfer coefficient were adjusted to match the temperature profile. Then the activation energy and pre-exponential factor of the reforming reaction were adjusted to align the flow rate more closely. Next, the activation energy and pre-exponential factor of the methanol decomposition reaction were adjusted to fit the mole fraction of CO better. Altering the rates of reaction causes the conversion to change, changing the energy demands. Thus, one sequentially adjusts the temperature steps and then the rate parameters, and then iterates until convergence is achieved. The results of that process are shown in Fig. 1 with the simulation represented by the continuous dashed line overlayed on the data extracted from [17].

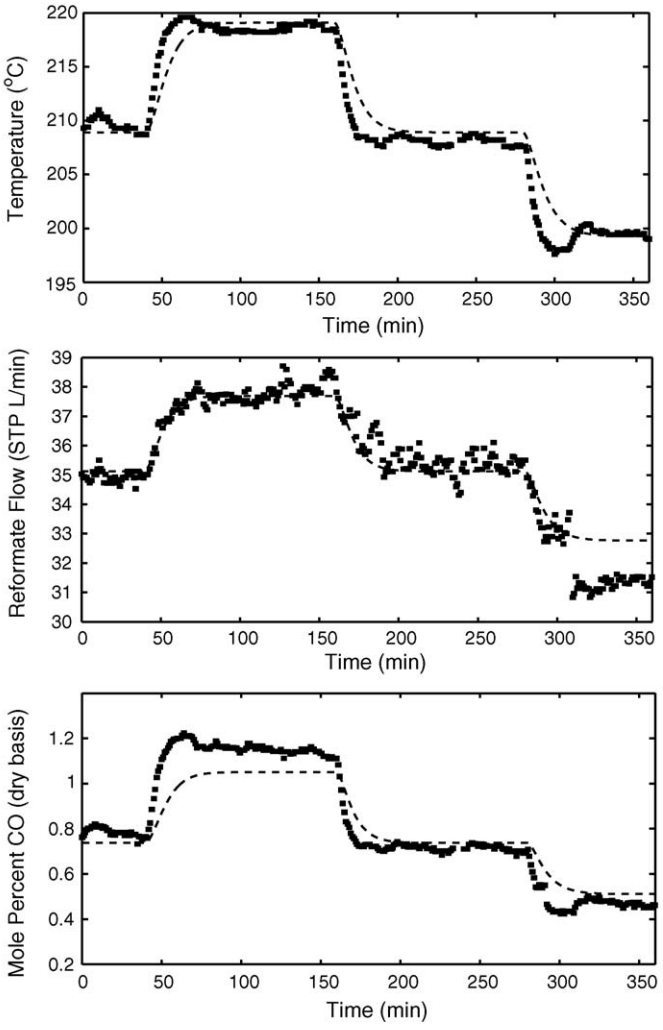

Fig. 1. Reformer model reproducing the temperature, flow rate, and mole percent CO profile data from Dams et al. [17].

2.2. PEMFC stack

In addition to the methanol reformer, a model is needed to simulate a fuel cell stack. Significant work has been done recently to create very detailed models of individual fuel cells and fuel cell stacks that take into account channel and flow-field geometries and model micro- and meso-scale transport phenomena, for instance Shimpalee et al. [45], Ferng et al. [20], and Guvelioglu and Stenger [22]. Computational fluid dynamics (CFD) based models are very complex, with most requiring parallel methods to find steady-state solutions, let alone real-time dynamic simulations. These types of models provide a great deal of insight into transport-dominated phenomena such as current and water distributions inside a single PEMFC or stack; they are quite valuable for improving cell and stack flow channel designs. However, CFD approaches are more detailed than what is required for balance-of-plant design schemes. These procedures mainly require a correlation between load and cell/stack voltage, mass flows, and average stack and stream temperatures. Nevertheless, these correlations are generally based on preceding experimental and mechanistic modeling work.

At the core of a fuel cell system is the membrane electrode assembly (MEA). Understanding the physical and chemical behavior of the MEA is crucial to the successful development of a fuel cell model, but it has not been a simple task. At the minimum, one must consider multi-component diffusion through porous media, electrochemical kinetics such as the reduction of oxygen in the cathode catalyst layer, as well as proton and water transport through the electrolyte membrane. Consequently, a great deal of effort has been made to better understand these phenomena within the last 10–15 years [9,10,36,46,25,19,53,54,43].

As the technology and expertise regarding fuel cells increased, models began to appear that were specific to particular hardware. Amphlett et al. developed a rather thorough model of the Ballard Mark IV PEMFC using both mechanistic [4] and empirical [5] approaches. The same group was also one of the

first to attempt a dynamic PEMFC model [8]. Their efforts in dynamic modeling were later improved upon by Wöhr et al. [50]. Using experience gained from modeling a number of different fuel cells, Mann et al. [31] developed a generalized steady state electrochemical model of a PEMFC that can be adjusted for individual cell parameters such as active membrane area and membrane thickness. Very recently, yet another dynamic fuel cell model has been published by Shan and Choe [44].

Finally, the knowledge base developed for modeling individual fuel cells has been combined to model entire fuel cell stacks. Much of the behavior of the overall stack is still related to the electrochemistry and transport within the MEA, but greater difficulties are encountered in the areas of heat and water management. Since stack models are typically used for system-level applications, much of the spatial detail is not needed. Additionally, the most detailed MEA and individual fuel cell models are often very computationally intensive, which would be further compounded as multiple cell models are combined into a stack. Therefore, a number of system-level models have been developed in which area- or volume-averaged quantities are used in addition to empirical correlations in order to make the stack models more tractable. An early example of this formulation was published by Amphlett et al. [6]. This approach was used by Yerramalla et al. [52] in their dynamic fuel cell model. Ceraolo et al. [14] have also developed a dynamic fuel cell model based on the underlying physical phenomena, but simplified enough to allow integration into larger system-level simulations. Recently, a dynamic PEMFC model was developed by Blackwelder [11] that can be integrated into the University of South Carolina's virtual test bed (VTB) design suite.[1] Finally, Xue et al. and Pathapati et al. [51,38] have developed a relatively simple system-level dynamic PEMFC stack model. While this model lacks the detailed spatial information and mechanistic transport behaviors, it performs suitably well for overall material and energy flows as well as stack voltage with relatively minimal computational demand.

2.2.1. Model formulation

Ultimately, the model presented simultaneously by Xue et al. [51] and Pathapati et al. [38] was selected for implementation, since it possessed the desired characteristics: dynamic treatment of cell/stack voltage, thermal behavior, and material flows in a relatively simple formulation. There are a total of seven states in the model.

- Masses of N_2 and O_2 (idealized air) in the cathode as well as H_2 in the anode (3).
- Enthalpies/temperatures of the anode and cathode volumes and the stack body (3).
- Dynamic activation overpotential V_{act} due to the charge double-layer capacitance effect (1).

The mass balances are very simple, since the anode and cathode are considered to be two well-mixed volumes with a single composition for each. The balance equations are of the general form:

$$\frac{dm_i}{dt} = \dot{m}_{i,in} - \dot{m}_{i,out} - \dot{m}_{i,diff} \tag{26}$$

where $\dot{m}_{i,in}$ and $\dot{m}_{i,out}$ are the inlet and outlet mass flow rates of species x through flow channels and $\dot{m}_{i,diff}$ is the flow rate of reactive species x (H_2 and O_2) into the MEA. The assumption is made that the diffused species are consumed quickly once they enter the MEA, so that the rates of diffusion can be determined stoichiometrically from the current being drawn on the stack, which is given by the following equation:

$$\dot{m}_{i,diff} = M_i \frac{I}{\nu_i \mathcal{F}} N \tag{27}$$

Note that M_i is the molecular weight of species i, I the current drawn on the stack, ν_i the stoichiometric factor between the number of moles of species i and the number of moles of electrons consumed in the reaction (2 for H_2 and 4 for O_2), $\mathcal{F}$ is Faraday's constant, and N is the number of cells in the stack.

The inlet and outlet flow rates are given by a combination of a simplified linear nozzle correlation and the ideal gas law. The nozzle correlation assumes that the volumetric flow rate across a valve is proportional to the pressure drop across the valve as the following equation:

$$\dot{V} = k_v \, \Delta P \tag{28}$$

Using the ideal gas law, the volumetric flow rate is converted to a molar flow rate, which yields a mass flow rate by use of the molecular weight:

$$\dot{m}_{i,in/out} = k_v \, \Delta P \, \frac{P}{RT} \, M_i \tag{29}$$

For consistency, the pressure P and temperature T are always assumed to be that of the upstream side of the valve. This flow formulation is one of the few differences from the published form of the model. In [51,38], the mass flow rate instead of the volumetric flow rate was specified to be proportional to the pressure drop. While that may be shown for pure gasses or fixed-composition gas mixtures, this assumption seems rather dubious. Under ideal gas conditions, the same number of moles (equivalently volume at fixed T, P) should pass through a valve for a given pressure drop, relatively independently of the composition. Hence the mass flow rate may vary considerably with composition, but the volumetric flow rate should not. Given that the composition of the cathode changes with the electrical load, it seems more appropriate to use a volume-based flow correlation. The anode mass balance has been modified similarly to include CO_2 as an inert gas that is part of an idealized reformate mixture.

The energy balances are nearly as rudimentary. In the anode, the balance is written:

$$\frac{dE_{an}}{dt} = (hA)_{an,s}(T_s - T_{an}) + \dot{m}_{H_2,in} H_{H_2,in} - \dot{m}_{H_2,out} H_{H_2,out} - \dot{m}_{H_2,diff} H_{H_2,diff} \tag{30}$$

where $(hA)_{an,s}$ is a lumped term containing the convective heat transfer coefficient and convective transfer area between the an-

[1] http://www.vtb.engr.sc.edu.

ode and the stack body, and the H_{H_2} terms are the specific enthalpies of the hydrogen gas streams flowing into the anode, out of the anode, and diffusing into the MEA. With the ideal gas assumption and a constant heat capacity approximation, the specific enthalpy for hydrogen gas relative to an arbitrary reference state is:

$$H_{H_2}(T) = H_{H_2,\mathrm{ref}} + C_{p,H_2} \quad (T - T_{\mathrm{ref}}) \tag{31}$$

where C_{p,H_2} is the constant-pressure specific heat capacity of hydrogen gas. A convenient choice for the reference state is at 298.15 K where $\Delta H_{f,H_2}$ is 0.0 J kg^{-1}. Thus, the specific enthalpy simplifies to:

$$H_{H_2}(T) = C_{p,H_2} \quad (T - 298.15) \tag{32}$$

Note that the enthalpy does not depend on pressure, due to the ideal gas assumption. The energy balance for the stack body has a few additional terms, namely convective heat loss to the surroundings:

$$\dot{E}_{s,\mathrm{loss}} = (hA)_{s,\mathrm{room}}(T_{\mathrm{room}} - T_s), \tag{33}$$

the heat from the electrochemical reaction to form water:

$$\dot{E}_{s,\mathrm{rxn}} = \dot{m}_{H_2,\mathrm{diff}}\, \Delta H_{\mathrm{rxn}} \tag{34}$$

(ΔH_{rxn} normalized per kilogram H_2 consumed), and energy loss equal to the rate of electrical energy production:

$$\dot{E}_{s,\mathrm{elec}} = -N\, V_{\mathrm{cell}} I \tag{35}$$

where again, N is the number of cells in the stack, V_{cell} the voltage across a single cell, and I is the current drawn on the stack. Finally, a generalized stack cooling term has been added to the original model to allow for the removal (or addition) of heat to maintain the stack body at a desired temperature. It is of the form:

$$\dot{E}_{s,\mathrm{cool}} = \dot{Q}_{\mathrm{cool}} \tag{36}$$

where $\dot{Q}_{\mathrm{cool}}$ becomes an additional adjustable input to the model. This allows for the construction of a control loop to regulate stack temperature, although it does not specify the form or geometry of any cooling solution.

The remaining dynamic state of this fuel cell model is the activation overpotential V_{act}. It is primarily due to the slow kinetics of oxygen reduction in the cathode catalyst layer. By theoretically analyzing the physical phenomena responsible for this effect, the overpotential was determined to be largely a function of temperature, the current density drawn from the cell, and the effective concentration of oxygen in the cathode catalyst layer, $c^*_{O_2}$. Using this knowledge, a steady state empirical correlation was constructed for the activation overpotential, given by the following equation:

$$\eta_{\mathrm{act}} = \xi_1 + \xi_2 T + \xi_3 T \ln i + \xi_4 T \ln c^*_{O_2} \tag{37}$$

While this correlation works well under steady state conditions, there is an additional dynamic effect due to the charge double layer capacitance, which arises due the buildup of charge at the membrane/electrode interface. By visualizing the stack as an equivalent circuit, a differential equation can be written for the activation overpotential, as shown in the following equation:

$$\frac{\mathrm{d}V_{\mathrm{act}}}{\mathrm{d}t} = \frac{I}{C} - \frac{V_{\mathrm{act}}}{R_{\mathrm{act}}\, C} = \frac{I}{C}\left(1 - \frac{V_{\mathrm{act}}}{\eta_{\mathrm{act}}}\right) \tag{38}$$

Additionally, there are ohmic losses in the stack predominantly related to transport processes. These losses are found to depend mainly on temperature and current density and have also been previously determined to obey an empirical relationship [4,5] of the form

$$R_{\mathrm{ohm}} = \xi_5 + \xi_6 T + \xi_7 i. \tag{39}$$

Finally, the cell voltage V_{cell} is calculated:

$$V_{\mathrm{cell}} = V_{\mathrm{Nernst}} - V_{\mathrm{act}} - i R_{\mathrm{ohm}} \tag{40}$$

where V_{Nernst} is a Nernstian relationship for the equilibrium cell potential dependent on temperature and the partial pressures of hydrogen and oxygen. The reader is referred to [51,38] and references therein for a more complete treatment of the PEMFC equations.

2.2.2. Simulink® implementation

Given its simplicity, the decision was made to implement the PEMFC model directly within Matlab® for its ease of use instead of native code algorithms such as LSODA [26,41]. To provide some performance enhancement, the ODEs of the model were implemented as a compiled C-MEX S-function. A variety of process inputs and model parameters were left exposed externally in order to be adjusted rapidly within the Simulink® environment without recompiling. In addition to the seven states in the model, a number of other useful quantities were output from the model, including anode/cathode pressures, stack voltage, and inlet/outlet mass flow rates.

The model requires volumes for the cathode and anode channels in order to compute the respective mass balances. However, for the purpose of performance and power scaling, the membrane area is the critical parameter. Therefore, considering the envisioned use for an optimal design problem, the worksheet specifies a cell membrane area and number of cells in the stack and then assumes constant volume/total area ratios to calculate the volumes of the anode and cathode. For the test cases presented in the work of Xue et al. and Pathapati et al. [51,38], the cathode was specified with a volume twice that of the anode. That ratio is preserved in this worksheet. Based on rough geometrical arguments, the ratio for the anode was calculated to be 0.2 and 0.4 cm^3 cm^{-2} for the cathode. Similarly, the weight of the stack is computed based on the cell membrane area and number of cells. Additionally, the current density drawn from a stack is more informative than the actual current, so the load on the stack is specified in terms of current density and then multiplied by the membrane area to determine the actual loads on the PEMFC stack.

2.3. Heat exchanger

Due to the differing operating temperatures between different components within the system, it will be necessary to heat and

cool a number of different process streams. In order to improve efficiency, it is possible to use excess heat from a hot stream such as the reformate to heat other streams such as the cathode air feed to the reformer stack. Cross-flow heat exchanger geometries are common for gas–gas heat exchange, so a simple steady state heat exchanger model is used.

Assuming uniform velocity profiles and constant physical properties, the governing equations for the heat exchanger can be made dimensionless with the solution depending solely on the Nusselt numbers on the hot and cold sides of the heat exchanger. The dimensionless problem was discretized using finite differences and solved off-line for combinations of Nusselt numbers ranging from 10^{-2} to 10^{2}. The dimensionless average hot and cold outlet temperature were tabulated for each case, allowing the heat exchanger to be implemented in simulation as a look-up table.

2.4. Auxiliary power source

While fuel cell stacks are typically able to respond to large variations in load or power quickly, the time scales of the fuel processing system are generally at least two orders of magnitude slower. Therefore, the rate at which the load can be increased on a PEMFC stack coupled to a fuel processor is limited by the rate at which hydrogen production can be increased. Consequently, some form of auxiliary power will be required to ensure satisfactory vehicle performance under normal operating conditions.

The selection of a specific auxiliary power source, such as lead-acid batteries or supercapacitors, is beyond the current scope of this work. Therefore the system-level model developed treats the auxiliary power source as a black-box component. It is assumed that this power source operates at a constant bus voltage – 120 V for this work – and is instantaneously able to provide enough current to provide the difference between the desired power and the PEMFC stack power. When the PEMFC is producing more power than is required, the excess is then used to recharge the auxiliary power unit. Furthermore, there is assumed to be a 5% loss in each direction (charging/discharging) as part of the power conversion process. One is then able to observe the amount of auxiliary capacity needed for a particular system configuration and power profile. The amount of capacity and the rate at which it is drawn can then be used to determine what type of auxiliary power source is most suitable for the application.

3. System-level integration and control

The components of the overall system model were connected as shown in Fig. 2 using Matlab® and Simulink®. This diagram depicts an open-loop configuration. By specifying material flow rates, operating temperatures and pressures, and the load on the stack, outputs such as stack power and hydrogen production can be observed. However, this is not the desired mode of operation. For vehicular operation, it is necessary to specify a desired power level and then have controllers on the system adjust stack load and hydrogen production to meet that goal. For this work, an idealized driving power profile was developed and is shown in Fig. 3. Although a true power profile would vary much more

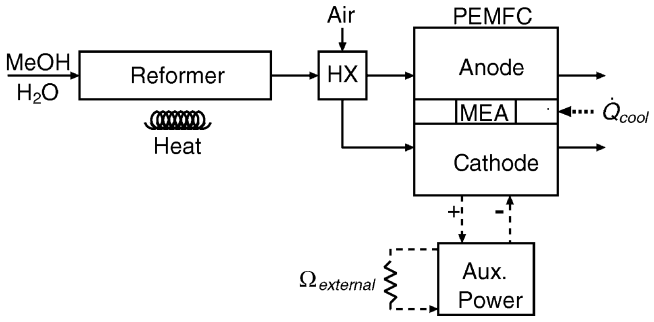

Fig. 2. Integrated system layout for the reformer/PEMFC stack system.

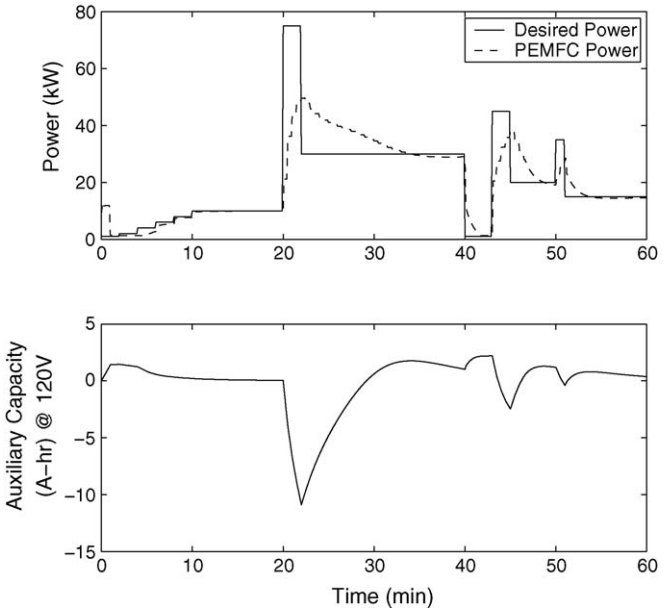

Fig. 3. Performance of system following the designated power profile. The parameter set for this run is $\{L_{ref} = 0.8,\ R_{ref} = 0.07,\ A_{mem} = 900,\ T_{sp,ref} = 550,\ T_{sp,stack} = 355\}$. Upper: PEMFC power compared to the desired system power. The auxiliary power at any time is the difference between the desired power and the PEMFC power. Lower: relative change in capacity of the auxiliary power system at the operating voltage of 120 V.

frequently, this profile is of the correct magnitude and attempts to account for warm-up, acceleration, braking, and cruising.

Several control loops are necessary to achieve satisfactory closed-loop operation. Two low-level regulatory proportional-integral (PI) feedback control loops provide temperature control on the reformer and the PEMFC stack. The reformate temperature can be controlled by the manipulation of the reformer wall temperature. In actual practice, the wall temperature is not the true manipulated variable; it would likely be a valve controlling fuel flow to a burner element. Similarly, the temperature of the PEMFC is maintained by adjusting the fictitious $\dot{Q}_{cool}$ term. In practice, the temperature would be regulated by adjusting the flow rate of a cooling liquid. Since the cooling fluid could never be used to heat the stack, the output of the PI controller passes through a saturation block to disallow values of $\dot{Q}_{cool}$ that add heat to the stack. Tunings for the controller gains K_c and the integral time constant τ_I are given in Table 2.

Two additional loops have the greatest impact on the performance of the closed-loop system. The first is the regulation of the

methanol flow rate into the reformer system. The second is the regulation of the load on the PEMFC. The manipulation of both quantities is based on the difference between the desired system power and the PEMFC stack power. For the sake of simplicity, these controllers were also modified forms of PI controllers. Ultimately, the implementation was more nuanced for several reasons. First, the power response of the PEMFC displays direct feedthrough since,

$$P_{\text{stack}} = i\, A_{\text{mem}}\, V_{\text{stack}}. \tag{41}$$

This direct feedthrough seemed to induce instabilities except at extremely low controller gains when using a standard PI formulation, most likely due to the large gain on the direct feedthrough. In order to mitigate the impact of the direct feedthrough (and equivalently step changes in the setpoint), the error signal ($P_{\text{sp}} - P_{\text{stack}}$) is first passed through a first order filter before reaching the controller. Thus, the control law is of the form:

$$i(s) = K_{\text{c}} \left(1 + \frac{1}{\tau_{\text{I}}\, s}\right) \frac{1}{\tau_{\text{f}}\, s + 1} (P_{\text{sp}}(s) - P_{\text{stack}}(s)), \tag{42}$$

where s is the Laplace variable. The control structure is identical for the methanol flow controller. For the power controller, a filter time constant of 0.1 min was selected, while a larger value of 2 min was used for the methanol flow rate, given the slower response of that component. Additionally, the power setpoint P_{sp} was more complicated than simply the desired power output at a given time. It was desired to operate the system so that the auxiliary power source remained as close to a reference charge level as possible. By integrating the load on the auxiliary power source, it was possible to track the relative change in capacity of that system. This auxiliary capacity level was then used to adjust the power setpoint according to the following linear feedback law:

$$P_{\text{sp}} = P_{\text{desired}} + K_{\text{aux}}\, C_{\text{aux}}. \tag{43}$$

For power measured in Watts and capacity in A h, a feedback proportionality constant K_{aux} of $-1000\,\text{W}\,(\text{A h})^{-1}$ provided satisfactory response without substantial oscillation in the auxiliary capacity level. Finally, actuator limits were placed on the control actions in accordance with physical limits. The methanol flow rate and load on the fuel cell stack cannot be lower than $0\,\text{L min}^{-1}$ and $0\,\text{A cm}^{-2}$. The maximum methanol flow rate was established as $1\,\text{L min}^{-1}$, which was somewhat arbitrary, but intentionally left rather high. Finally, the MEAs in the PEMFC stack can be damaged if the unit is starved of hydrogen, so there is a dynamic upper limit on PEMFC load, preventing the load from exceeding that needed to consume 85% of the hydrogen being produced by the reformer. Representative control action for these two controllers is shown in Fig. 4.

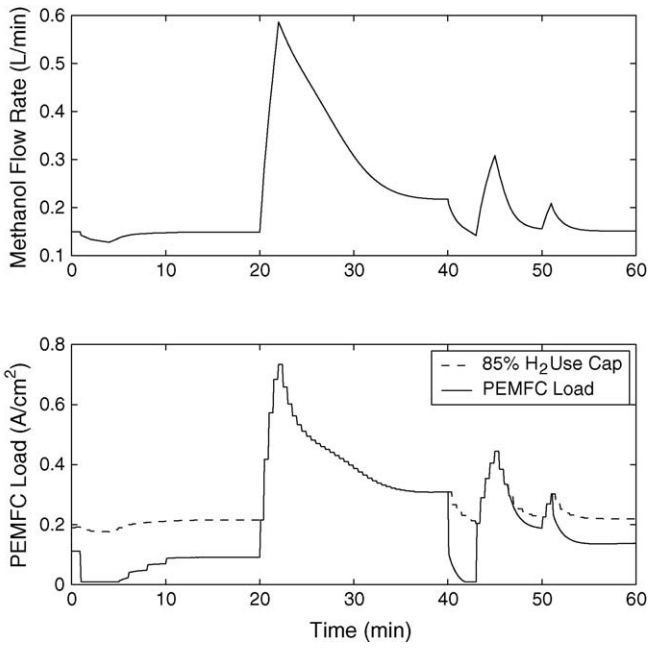

Fig. 4. Control actions taken by the major system controllers corresponding to the desired power trajectory shown in Fig. 3. The parameter set for this run is $\{L_{\text{ref}} = 0.8,\ R_{\text{ref}} = 0.07,\ A_{\text{mem}} = 900,\ T_{\text{sp,ref}} = 550,\ T_{\text{sp,stack}} = 355\}$. Upper: liquid methanol flow rate into the reformer. The liquid water flow rate into the reformer is fixed at a 2:3 ratio to the methanol flow rate. Lower: load current density (solid) on the PEMFC stack as a function of time. The dynamic upper constraint (dashed) is the current density which would use 85% of the hydrogen output from the reformer.

4. Results and discussion

Simulation studies were performed to gauge the effects of various design and operational parameters on the overall performance of the system. There are a number of parameters that may influence operation, only five were chosen for consideration in this study. Three were design parameter related to the physical structure of the system: reformer length, reformer radius, and active membrane area for each cell of the PEMFC stack. The two additional parameters were operational in nature: the reformer outlet temperature setpoint and the PEMFC stack body temperature setpoint. Four values of each parameter were considered and are listed in Table 3. Values for the other parameters used in the system model are contained in Table 4.

Given 5 parameters, each with 4 possible values allows for 1024 different system configurations to be studied. For each pa-

Table 2
Control loop tuning parameters

Loop	K_{c}	τ_{I} (min)
Reformer temperature	$1\,\text{K K}^{-1}$	10
PEMFC temperature	$5\,\text{kJ K}^{-1}$	10
PEMFC load	$10^{-4}\,(\text{A cm}^{-2})\,\text{W}^{-1}$	1
MeOH flow	$10^{-5}\,(\text{L min}^{-1})\,\text{W}^{-1}$	2

Table 3
Parameter values studied in the sensitivity analysis

Parameter	1	2	3	4
Reformer length (m)	0.600	0.80	1.00	1.20
Reformer radius (m)	0.025	0.04	0.07	0.10
PEMFC membrane area (cm^2)	800	900	1000	1200
Reformer temperature setpoint (K)	500	550	575	600
PEMFC temperature setpoint (K)	335	345	355	365

rameter combination, the system is simulated trying to reproduce the hypothetical power profile shown in Fig. 3. No effort is made to tune the control loops for each configuration. Consequently, the system response for each configuration may not be ideal. In fact, results were not obtained for several configurations, due to numerical difficulties, possibly resulting from controller tunings being unstable at the given configuration. Nevertheless, system performance was analyzed based on factors including total methanol usage, hydrogen utilization percentage, auxiliary power capacity range, and a gross efficiency measure for all configurations for which results are available.

Fig. 5 is a histogram of the net methanol usage for the various system parameter combinations over the one hour reference power trajectory. Note that the distribution appears bimodal with a large normal-looking distribution centered around 11 L and a smaller peak distributed between about 6.5 and 8.0 L. By analyzing the parameter combinations that were found in the second peak, it was found that all were at the lowest value of the reformer setpoint temperature: 500 K. Intuition indicates that lower methanol usage should be a positive characteristic for a design, but system design must consider a variety of factors. Before reaching any conclusions, it is necessary to examine the performance of these parameter configurations in the other performance categories. The next category is hydrogen utilization. For this analysis, hydrogen utilization is reported as the percentage of hydrogen produced by the reformer that is consumed by a single pass through the PEMFC stack. In practice, it may be possible to run anode exhaust into a recycle loop or at least flare the remaining hydrogen to capture its energy as heat, but these options are not considered here. The distribution of hydrogen utilization over the parameter combinations is shown in Fig. 6. Utilization is distributed widely between about 55% and 78% with a large grouping between 55% and 60%. Furthermore, it was found that the parameter combinations that were in the smaller peak for methanol utilization were also the combinations that had greater than 70% hydrogen utilization. Once again, it would appear that high hydrogen utilization would be a positive design characteristic.

However, the picture changes dramatically when auxiliary power capacity is considered. Fig. 7 illustrates the distribution of auxiliary power capacity for the various combinations. Once again, there is a very wide range of results between about 10 and 120 A h at 120 V operating voltage with a significant number (58%) below 20 A h. The amount of surge power needed in the system is very critical to the overall design, since it strongly influences both the weight and the cost of the system. This bodes poorly for the low methanol consumption/high hydrogen utilization parameter combinations, since they were the ones which required 80 A h and higher of auxiliary capacity. This represents at least a four- to six-fold increase over the majority of the other configurations, and suggests that these particular designs are inadequate.

Finally, the histogram of gross efficiencies is presented in Fig. 8. For this study, the gross efficiency was considered to be the sum of the electrical output of the PEMFC stack and the change in the electrical energy of the auxiliary power divided by the higher heating value of the methanol consumed (17,990 kJ L^{-1}).

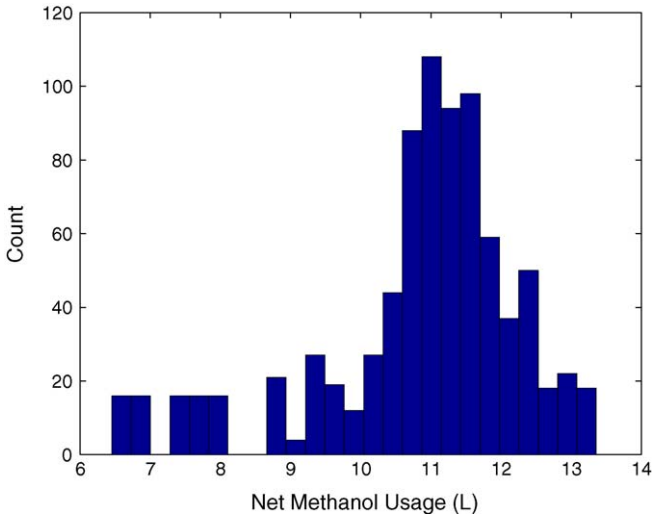

Fig. 5. Histogram of methanol usage for the various parameter configurations following the reference power trajectory shown in Fig. 3. Net usage is computed assuming that 95% of unreacted methanol leaving the reformer can be recaptured and reused.

Table 4
Other system operational parameters

Parameter	Value
Number of cells (#)	120
Aux. power voltage (V)	120
PEMFC cathode pressure (atm)	3.0
Reformer pressure (atm)	2.0
Reformer heat transfer coefficient (J m^{-2} s K)	50.0
Liquid MeOH/H_2O ratio (v/v)	3 : 2
HX height (m)	0.10
HX cold length (m)	0.15
HX hot length (m)	0.10
HX channels/side (#)	5
HX hot channel C_p (J mol^{-1} K)	36.0
HX cold channel C_p (J mol^{-1} K)	28.0
HX heat transfer coefficient (J m^{-2} s K)	50.0

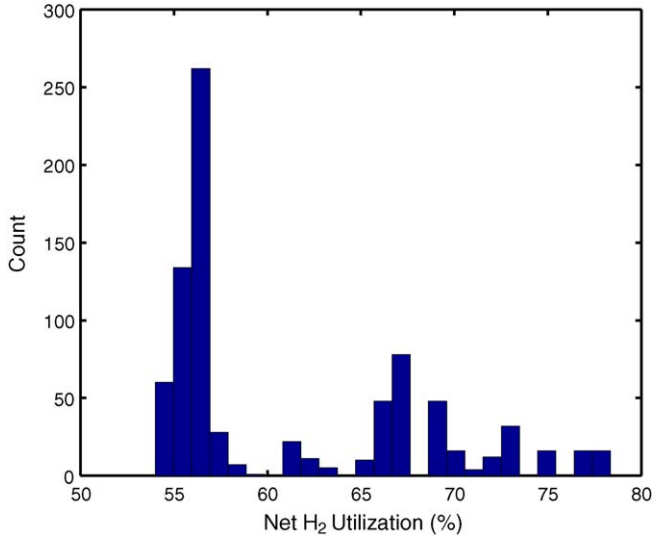

Fig. 6. Histogram of hydrogen utilization for the various parameter configurations following the reference power trajectory shown in Fig. 3.

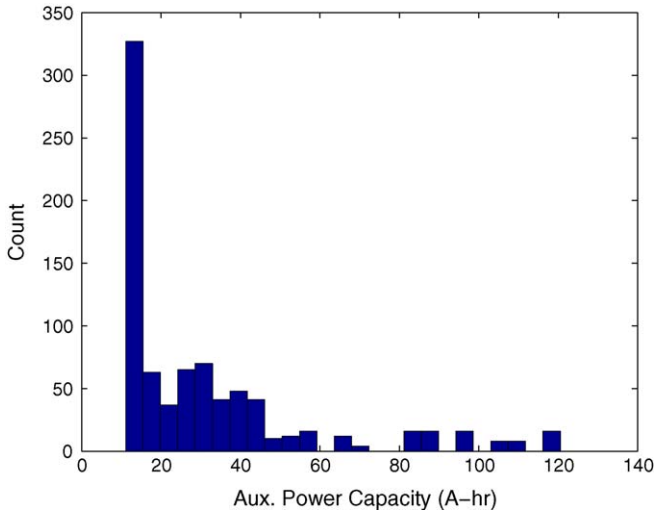

Fig. 7. Histogram of the necessary sizing of the auxiliary power capacity needed for the various parameter configurations to follow the reference power trajectory shown in Fig. 3.

There are a number of factors not considered in this measure, including the heat of vaporization for the methanol and water feed to the reformer, the external heat to drive the reactions in the reformer, the heating value of the hydrogen in the PEMFC anode exhaust, and other ancillary costs such as pumping costs and work to cool the PEMFC stack. Consequently, these numbers should not be viewed as an absolute quantitative measure, but rather a relative scale to compare performance among various parameter combinations. Most of the results are normally distributed around an efficiency value of about 36%, but again there is an extended lower tail. As expected, the low methanol use combinations comprise the lower tail in the range of 20–30%.

More insight is gained by examining the dynamic profile of these low methanol consumption cases. It is apparent that at low reformer operating temperatures, the conversion of methanol to hydrogen is very low, regardless of the methanol flow rate, resulting in the low net methanol usage. Thus, due to the control constraints based on hydrogen flow, the load on the PEMFC stack is kept low and cannot meet the power demand at most times. Even when using most of the available hydrogen, the system is forced to draw heavily on the auxiliary power unit, which is why these configurations required much more auxiliary capacity. Finally, even at the end of duty cycle, these configurations were not able to recharge the auxiliary capacity to its initial level. This net loss of energy from the auxiliary power unit results in the lowered efficiencies of these designs, and further indicates that they would not be good choices for a vehicular power system.

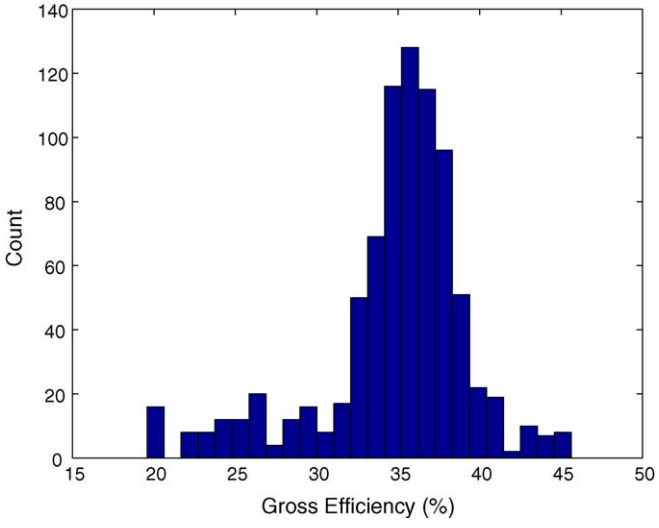

Fig. 8. Histogram of the gross efficiency measure for the various parameter configurations when following the reference power trajectory shown in Fig. 3.

5. Future work

This work begins to quantify the performance tradeoffs that result from design and operational decisions for the methanol reformer/PEMFC system. There are a number of avenues to explore this work further. System performance can be studied for different equipment configurations. Model improvements and additions can be incorporated. Currently, components such as the reformer feed evaporator and any reformate processing such as preferential oxidation are not considered, and while they would be expected to significantly impact the dynamics of the process, would give a more accurate estimate of fuel and energy efficiency for the system. Additionally, the representative power profile used to drive the system is very simplistic. Eventually it would be useful to consider a power profile that is more realistic. By making certain assumptions about the mass and drag of the vehicle, it is possible to take driving schedules such as the federal urban driving schedule (FUDS) or the federal highway driving schedule (FHDS), which specify velocities, and calculate power profiles. Since the mass of the vehicle depends on the size of the main components, the power profile should be adjusted accordingly for each configuration. Ogden et al. have a clear demonstration of this approach [37].

Furthermore, the sensitivity studies were only conducted with five parameters and four values for each parameter. It is therefore unlikely that any of the exact parameter combinations explored here will be optimal in any of the performance metrics. Given that there are a number of different objectives to consider when designing such a power plant including cost, weight, size, and efficiency, this model could be used as part of an multiobjective optimization procedure. One approach would be to develop a single composite objective function, which is a weighted combination of the objectives under consideration, similar to:

$$\Phi = \Gamma_{\text{cost}}\varphi_{\text{cost}} + \Gamma_{\text{size}}\varphi_{\text{size}} + \Gamma_{\text{mass}}\varphi_{\text{ma ss}} - \Gamma_{\text{eff}}\varphi_{\text{eff}}. \quad (44)$$

In order to achieve this, one would also need to establish correlations between the easily calculated performance measures such as auxiliary power capacity and the design objectives such as monetary cost, system size (volume), and system mass. Also, there can be considerable difficulty in choosing appropriate values for the weighting factors Γ_i that produce a satisfactory result. It may be possible to use techniques from Pareto multiobjective optimization theory to obtain these values.

Additionally, any optimization-based approaches that include dynamic simulations as part of the objective function raise legitimate concerns about the computational demands of the method.

However, any optimization techniques that use finite differencing schemes to obtain gradients or otherwise need to evaluate multiple independent points in the solution space can benefit from parallel computing techniques. For instance, for a function of N different variables, $N + 1$ points need to be evaluated to compute the gradient at a single point; once these points are chosen, each can be evaluated independently without knowledge of the values at any other points. Thus, this sort of operation is well-suited for parallelization, and can make a significant impact on the time necessary for optimization calculations [13,24].

Clearly, the development of liquid-fueled vehicular fuel cell power plants is a very active area for ongoing research, both in the fundamental theoretical understanding of the processes involved and the application of techniques for design and integration.

6. Conclusions

This work describes the development and implementation of a system level model of a vehicular reformer/PEMFC stack power system. Particular emphasis has been placed on the interconnections between sub-units and the formulation of control loops to operate the system to meet desired power targets. With a particular hardware configuration, a sensitivity study was conducted to determine the influence of various design and operating parameters on system performance. Specifically, it was shown that the operation of the reformer at low temperatures gives particularly inferior performance. Recommendations for a particular design have not yet been made, since they are very sensitive to the relative importance of the performance metrics, but doing so remains a future objective. Nevertheless, a useful model framework has been developed for the dynamic analysis of a complex integrated system.

References

[1] Annual Energy Review 2003. Technical Report DOE/EIA-0384(2003). US Dept. of Energy—Energy Information Administration, Washington, DC, 2004.

[2] J. Agrell, H. Birgersson, M. Boutonnet, I. Melián-Cabrera, R.M. Navarro, J.L.G. Fierro, Production of hydrogen from methanol over Cu/ZnO catalysts promoted by ZrO_2 and Al_2O_3, J. Catal. 219 (2003) 389–403.

[3] J. Agrell, M. Boutonnet, J. Fierro, Production of hydrogen from methanol over binary Cu/ZnO catalysts. Part II. Catalytic activity and reaction pathways, Appl. Catal. A: Gen. 253 (2003) 213–223.

[4] J. Amphlett, R. Baumert, R. Mann, B. Peppley, P. Roberge, T. Harris, Performance modeling of the ballard mark IV solid polymer electrolyte fuel cell. I. Mechanistic model development, J. Electrochem. Soc. 142 (1) (1995) 1–9.

[5] J. Amphlett, R. Baumert, R. Mann, B. Peppley, P. Roberge, T. Harris, Performance modeling of the ballard mark IV solid polymer electrolyte fuel cell. II. Empirical model development, J. Electrochem. Soc. 142 (1) (1995) 10–15.

[6] J.C. Amphlett, R.M. Baumert, R.F. Mann, B.A. Peppley, P.R. Roberge, A. Rodrigues, Parametric modeling of the performance of a 5-kW proton exchange membrane fuel cell stack, J. Power Sources 49 (1994) 349–356.

[7] J.C. Amphlett, K.A.M. Creber, J.M. Davis, R.F. Mann, B.A. Peppley, D.M. Stokes, Hydrogen production by steam reforming of methanol for polymer electolyte fuel cells, Int. J. Hydrogen Energy 19 (2) (1994) 131–137.

[8] J.C. Amphlett, R.F. Mann, B.A. Peppley, P.R. Roberge, A. Rodrigues, A model predicting transient responses of proton exchange membrane fuel cells, J. Power Sources 61 (1996) 183–188.

[9] D.M. Bernardi, M.W. Verbrugge, Mathematical model of a gas diffusion electrode bonded to a polymer electrolyte, AIChE J. 37 (8) (1991) 1151–1163.

[10] D.M. Bernardi, M.W. Verbrugge, A mathematical model of the solid polymer electrolyte fuel cell, J. Electrochem. Soc. 139 (9) (1992) 2477–2491.

[11] M.J. Blackwelder, System-level model of a polymer electrolyte membrane fuel cell stack. PhD Thesis, University of South Carolina, Columbia, SC 29208, 2005.

[12] K.M. Vanden Bussche, G.F. Froment, A steady-state kinetic model for methanol synthesis and the water gas shift reaction on a commercial $Cu/ZnO/Al_2O_3$ catalyst, J. Catal. 161 (1996) 1–10.

[13] R. Byrd, R. Schnabel, G. Schultz, Parallel quasi-Newton methods for unconstrained optimization, Math. Prog. 42 (1988) 273–306.

[14] M. Ceraolo, C. Miulli, A. Pozio, Modelling static and dynamic behavior of proton exchange membrane fuel cells on the basis of electro-chemical description, J. Power Sources 113 (2003) 131–144.

[15] D.J. Chmielewski, Y. Hu, D.D. Papadias, Start-up and feedback control of autothermall reforming reactors, in: Proceedings of the AIChE Annual Meeting, 2005.

[16] A.P. Colburn, A method of correlating forced convection heat transfer data and a comparison with fluid friction, Trans. Am. Inst. Chem. Eng. 29 (1933) 174–210.

[17] R.A.J. Dams, P.R. Hayter, S.C. Moore. Continued Development of a Mathematical Model for a Methanol Reformer, Technical Report ETSU F/02/00152/REP, Wellman CJB Ltd., 2001.

[18] D. Doss, R. Kumar, R.K. Ahluwalia, M. Krumpelt, Fuel processors for automotive fuel cell systems: a parametric analysis, J. Power Sources 102 (1) (2001) 1–15.

[19] M. Eikerling, Yu.I. Kharkats, A.A. Kornyshev, Yu.M. Volfkovich, Phenomenological theory of electro-osmotic effect and water management in polymer electrolyte proton–conducting membranes, J. Electrochem. Soc. 145 (8) (1998) 2684–2699.

[20] Y.M. Ferng, Y.C. Tzang, B.S. Pei, C.C. Sun, A. Su, Analytical and experimental investigations of a proton exchange membrane fuel cell, Int. J. Hydrogen Energy 29 (2004) 381–391.

[21] H.S. Fogler, Elements of Chemical Reaction Engineering, Prentice-Hall, Upper Saddle River, New Jersey, 1999 3rd ed..

[22] G. Guvelioglu, H. Stenger, Computational fluid dynamics modeling of polymer electrolyte membrane fuel cells, J. Power Sources 147 (2005) 95–106.

[23] M.P. Harold, B. Nair, G. Kolios, Hydrogen generation in a Pd membrane fuel processor: assessment of methanol-based reaction systems, Chem. Eng. Sci. 58 (2003) 2551–2571.

[24] K.A. High, R.D. LaRoche, Parallel nonlinear optimization techniques for chemical process design problems, Comput. Chem. Eng. 19 (6/7) (1995) 807–825.

[25] J.T. Hinatsu, M. Mizuhata, H. Takenaka, Water upate of perfluorosulfonic acid membranes from liquid water and water vapor, J. Electrochem. Soc. 141 (6) (1994) 1493–1498.

[26] A.C. Hindmarsh, LSODE and LSODI: two new initial value ordinary differential equation solvers, ACM-Signum Newslett. 15 (4) (1980) 10–11.

[27] B. Höhlein, M. Boe, J. Bøgild-Hansen, P. Bröckerhoff, G. Colsman, B. Emonts, R. Menzer, E. Riedel, Hydrogen from methanol for fuel cells in mobile systems: development of a compact reformer, J. Power Sources 61 (1996) 143–147.

[28] R.-F. Horng, Transient behavior of a small methanol reformer for fuel cell during hydrogen production after cold start, Energy Convers. & Management 46 (2005) 1193–1207.

[29] A. Kulprathipanja, J.L. Falconer, Partial oxidation of methanol for hydrogen production using ITO/Al_2O_3 nanoparticle catalysts, Appl. Catal. A: Gen. 261 (1) (2004) 77–86.

[30] B. Lindström, L.J. Pettersson, Development of a methanol fuelled reformer for fuel cell applications, J. Power Sources 118 (2003) 71–78.

[31] R.F. Mann, J.C. Amphlett, M.A.I. Hooper, H.M. Jensen, B.A. Peppley, P.R. Roberge, Development and application of a generalised steady-state

electrochemical model for a PEM fuel cell, J. Power Sources 86 (2000) 173–180.
[32] Maplesoft, Maple Reference Guide, Springer Verlag, 2000.
[33] The MathWorks. Matlab® 6.5. Prentice Hall, 2002.
[34] P. Mizsey, E. Newson, T.B. Truong, P. Hottinger, The kinetics of methanol decomposition: a part of autothermal partial oxidation to produce hydrogen for fuel cells, Appl. Catal. A: Gen. 213 (2001) 233–237.
[35] E.B. Nauman, Chemical Reactor Design, Optimization and Scaleup, McGraw-Hill, New York, 2001.
[36] T.V. Nguyen, R.E. White, J. Electrochem. Soc. 145 (1149) (1993).
[37] J.M. Ogden, M.M. Steinbugler, T.G. Kreutz, A comparison of hydrogen, methanol, and gasoline as fuels for fuel cell vehicles: implications for vehicle design and infrastructure development, J. Power Sources 79 (2) (1999) 143–168.
[38] P.R. Pathapati, X. Xue, J. Tang, A new dynamic model for predicting transient phenomena in a PEM fuel cell system, Renew. Energy 30 (2005) 1–22.
[39] B.A. Peppley, J.C. Amphlett, L.M. Kearns, R.F. Mann, Methanol–steam reforming On $Cu/ZnO/Al_2O_3$ catalysts. Part 2. A comprehensive kinetic model, Appl. Catal. A: Gen. 179 (1999) 31–49.
[40] B.A. Peppley, J.C. Amphlett, L.M. Kearns, R.F. Mann, Methanol-steam reforming On $Cu/ZnO/Al_2O_3$. Part 1. The reaction network, Appl. Catal. A: Gen. 179 (1999) 21–29.
[41] L.R. Petzold, Automatic selection of methods for solving stiff and nonstiff systems of ordinary differential equations, SIAM J. Sci. Stat. Comput. 4 (1983) 136–148.
[42] S.S. Rao, Applied Numerical Methods for Engineers and Scientists, Prentice Hall, 2002 chapter 11, pp. 823–826.
[43] A. Rowe, X. Li, Mathematical modeling of proton exchange membrane fuel cells, J. Power Sources 102 (2001) 82–96.
[44] Y. Shan, S.-Y. Choe, A high dynamic PEM fuel cell model with temperature effects, J. Power Sources 145 (2005) 30–39.
[45] S. Shimpalee, S. Greenway, D. Spuckler, J.W. Van Zee, Predicting water and current distributions in a commercial-size PEMFC, J. Power Sources 135 (2004) 79–87.
[46] T.E. Springer, M.S. Wilson, S. Gottesfeld, Modeling and experimental diagnostics in polymer electrolyte fuel cells, J. Electrochem. Soc. 140 (12) (1993) 3513–3526.
[47] M. Turco, G. Bagnasco, U. Costantino, F. Marmottini, T. Montanari, G. Ramis, G. Busca, Production of hydrogen from oxidative steam reforming of methanol. II. Catalytic activity and reaction mechanism on $Cu/ZnO/Al_2O_3$ hydrotalcite-derived catalysts, J. Catal. 228 (2004) 56–65.
[48] R.E. Uhrig, Using plug-in hybrid vehicles to drastically reduce petroleum-based fuel consumption and emissions, The Bent of Tau Beta Pi, Spring (2005) 13–19.
[49] M. Wang, Fuel choices for fuel-cell vehicles: well-to-wheels energy and emission impacts, J. Power Sources 112 (2002) 307–321.
[50] M. Wöhr, K. Bowin, W. Schnurnberger, M. Fischer, W. Neubrand, G. Eigenberger, Dynamic modeling and simulation of a polymer membrane fuel cell including mass transport limitation, Int. J. Hydrogen Energy 23 (3) (1998) 213–218.
[51] X. Xue, J. Tang, A. Smirnova, R. England, N. Sammes, System level lumped-parameter dynamic modeling of PEM fuel cell, J. Power Sources 133 (2004) 188–204.
[52] S. Yerramalla, A. Davari, A. Feliachi, T. Biswas, Modeling and simulation of the dynamic behavior of a polymer electrolyte membrane fuel cell, J. Power Sources 124 (1) (2003) 104–113.
[53] J.S. Yi, T.V. Nguyen, An along-the-channel model for proton exchange membrane fuel cells, J. Electrochem. Soc. 145 (4) (1998) 1149–1159.
[54] J.S. Yi, T.V. Nguyen, Multicomponent transport in porous electrodes of proton exchange membrane fuel cells using the interdigitated gas distributors, J. Electrochem. Soc. 146 (1) (1999) 38–45.